



*Supplement of*

**Global simulation of dissolved  $^{231}\text{Pa}$  and  $^{230}\text{Th}$  in the ocean and the sedimentary  $^{231}\text{Pa} / ^{230}\text{Th}$  ratios with the ocean general circulation model COCO ver4.0**

**Yusuke Sasaki et al.**

*Correspondence to:* Akira Oka (akira@aori.u-tokyo.ac.jp)

The copyright of individual parts of the supplement might differ from the article licence.

Experiment	$^{231}\text{Pad}$	Global			$^{231}\text{Pap}$		
		slope	R	RMSD	slope	R	RMSD
Siddall_EXP		1.57 (1.88)	$5.76 \times 10^{-1}$ ( $7.24 \times 10^{-1}$ )	$2.51 \times 10^{-1}$ ( $1.47 \times 10^{-1}$ )	$9.91 \times 10^{-2}$ ( $6.60 \times 10^{-2}$ )	$1.91 \times 10^{-1}$ ( $1.00 \times 10^{-1}$ )	$1.41 \times 10^{-2}$ ( $1.59 \times 10^{-2}$ )
CTRL_EXP		$7.56 \times 10^{-1}$ (1.04)	$7.51 \times 10^{-1}$ ( $8.98 \times 10^{-1}$ )	$8.21 \times 10^{-2}$ ( $4.57 \times 10^{-2}$ )	$6.16 \times 10^{-2}$ ( $6.15 \times 10^{-2}$ )	$1.87 \times 10^{-1}$ ( $1.44 \times 10^{-1}$ )	$1.37 \times 10^{-2}$ ( $1.43 \times 10^{-2}$ )
3D_EXP		1.57 (1.88)	$5.76 \times 10^{-1}$ ( $7.24 \times 10^{-1}$ )	$2.51 \times 10^{-1}$ ( $1.47 \times 10^{-1}$ )	$9.91 \times 10^{-2}$ ( $6.60 \times 10^{-2}$ )	$1.91 \times 10^{-1}$ ( $1.00 \times 10^{-1}$ )	$1.41 \times 10^{-2}$ ( $1.59 \times 10^{-2}$ )

$^{230}\text{Thd}$	Global			$^{230}\text{Thp}$			Global		
	Slope	R	RMSD	Slope	R	RMSD	Slope	R	RMSD
Siddall_EXP	3.85 (4.44)	$7.10 \times 10^{-1}$ ( $8.68 \times 10^{-1}$ )	1.31 (1.17)	$3.50 \times 10^{-2}$ ( $1.26 \times 10^{-1}$ )	$1.79 \times 10^{-1}$ ( $2.35 \times 10^{-1}$ )	$2.45 \times 10^{-1}$ ( $8.56 \times 10^{-2}$ )			
KREF_EXP	$6.36 \times 10^{-1}$ ( $8.81 \times 10^{-1}$ )	$7.00 \times 10^{-1}$ ( $8.08 \times 10^{-1}$ )	$2.32 \times 10^{-1}$ ( $2.05 \times 10^{-1}$ )	$3.57 \times 10^{-2}$ ( $1.67 \times 10^{-1}$ )	$2.81 \times 10^{-1}$ ( $4.23 \times 10^{-1}$ )	$2.43 \times 10^{-1}$ ( $7.87 \times 10^{-2}$ )			
CTRL_EXP	$7.65 \times 10^{-1}$ ( $9.79 \times 10^{-1}$ )	$8.18 \times 10^{-1}$ ( $8.41 \times 10^{-1}$ )	$1.71 \times 10^{-1}$ ( $1.57 \times 10^{-1}$ )	$3.17 \times 10^{-2}$ ( $1.65 \times 10^{-1}$ )	$2.79 \times 10^{-1}$ ( $4.87 \times 10^{-1}$ )	$2.44 \times 10^{-1}$ ( $7.82 \times 10^{-2}$ )			
3D_EXP	1.22 (1.73)	$7.31 \times 10^{-1}$ ( $8.30 \times 10^{-1}$ )	$2.78 \times 10^{-1}$ ( $2.98 \times 10^{-1}$ )	$3.59 \times 10^{-2}$ ( $1.67 \times 10^{-1}$ )	$2.78 \times 10^{-1}$ ( $4.31 \times 10^{-1}$ )	$2.43 \times 10^{-1}$ ( $7.85 \times 10^{-2}$ )			

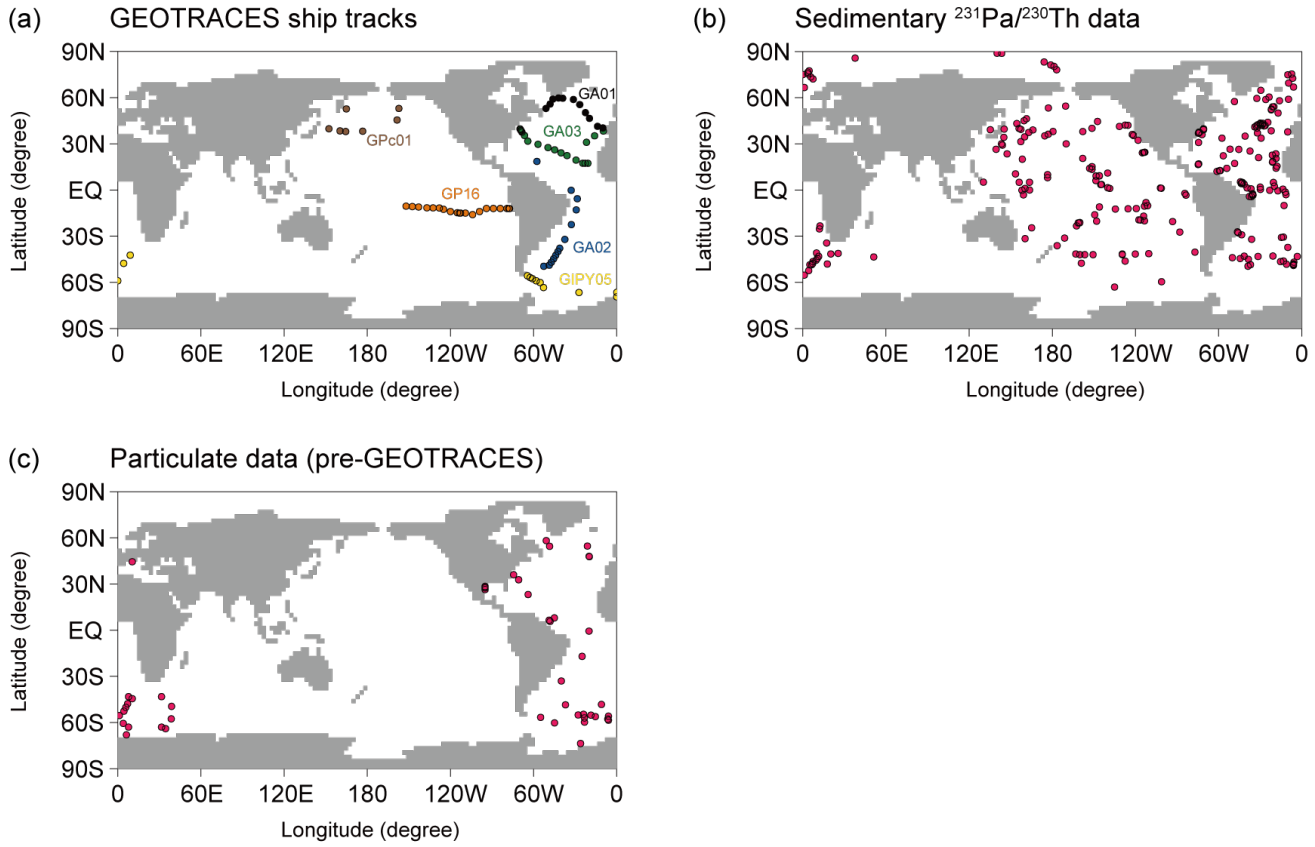
  

$^{231}\text{Pa}/^{230}\text{Th}$ (sediment)	Global			$^{231}\text{Pa}/^{230}\text{Th}$ (seawater)			Global		
	Slope	R	RMSD	Slope	R	RMSD	Slope	R	RMSD
Siddall_EXP	$2.71 \times 10^{-1}$	$3.46 \times 10^{-1}$	$5.03 \times 10^{-2}$				$1.61 \times 10^{-1}$	$2.48 \times 10^{-1}$	$6.64 \times 10^{-2}$
KREF_EXP	$4.21 \times 10^{-1}$	$4.21 \times 10^{-1}$	$5.74 \times 10^{-2}$				$3.40 \times 10^{-1}$	$2.11 \times 10^{-1}$	$1.08 \times 10^{-1}$
CTRL_EXP	$3.91 \times 10^{-1}$	$4.24 \times 10^{-1}$	$5.34 \times 10^{-2}$				$2.50 \times 10^{-1}$	$2.30 \times 10^{-1}$	$8.15 \times 10^{-2}$
3D_EXP	$4.73 \times 10^{-1}$	$4.42 \times 10^{-1}$	$5.42 \times 10^{-2}$				$3.30 \times 10^{-1}$	$1.71 \times 10^{-1}$	$1.33 \times 10^{-1}$

**Table S1.** Metrics of model-data misfits about  $^{231}\text{Pa}$  and  $^{230}\text{Th}$  simulated in our Siddall\_EXP, KREF\_EXP, CTRL\_EXP, and 3D\_EXP: the slope of linear regression (slope), the linear correlation coefficient (R), and the root mean square deviation (RMSD) of our experiment against all of the available data from GEOTRACES Intermediate Data Product 2017 (Schlitzer et al., 2018).  $^{231}\text{Pad}$ ( $^{230}\text{Thd}$ ) and  $^{231}\text{Pap}$ ( $^{230}\text{Thp}$ ) denote dissolved  $^{231}\text{Pa}$  ( $^{230}\text{Th}$ ) and particulate  $^{231}\text{Pa}$  ( $^{230}\text{Th}$ ), respectively. Values for  $^{231}\text{Pa}/^{230}\text{Th}$  ratios in sediments and water column are also shown in the table. For dissolved  $^{231}\text{Pa}$  and  $^{230}\text{Th}$ , we compared model results with the GEOTRACES data (GA02, GA03, GIPY05, GPc01 and GP16 sections). Numbers in parentheses of dissolved  $^{231}\text{Pa}$  and  $^{230}\text{Th}$  indicate comparisons only with the GEOTRACES GA02 data. For particulate  $^{231}\text{Pa}$  and  $^{230}\text{Th}$ , we compared model results with the GEOTRACES data (GA03, GIPY05, and GP16 sections). Numbers in parentheses of particulate  $^{231}\text{Pa}$  and  $^{230}\text{Th}$  indicate comparisons with pre-GEOTRACES data shown in Fig. S1c. For  $^{231}\text{Pa}/^{230}\text{Th}$  ratios in seawater, we compared model results with the GEOTRACES data (GA03, GIPY05, and GP16 sections). For  $^{231}\text{Pa}/^{230}\text{Th}$  ratios in sediment, the model results are compared with the sedimentary data shown in Fig. S1b.

Experiment	$^{231}\text{Pa}$	$^{230}\text{Th}$
Siddall_EXP	211	89
KREF_EXP	103	18
CTRL_EXP	103	21
3D_EXP	211	28

**Table S2.** The residence time of  $^{231}\text{Pa}$  and  $^{230}\text{Th}$  (year) simulated in our Siddall\_EXP, KREF\_EXP, CTRL\_EXP, and 3D\_EXP are displayed.



**Figure S1.** (a) Ship tracks of GEOTRACES data used in this study. (b) Sedimentary  $^{231}\text{Pa}/^{230}\text{Th}$  data obtained in pre-GEOTRACES studies (Mangianini & Sonntag, 1977; Müller & Mangini, 1980; Anderson et al., 1983; Shimmield et al., 1986; Schmitz et al., 1986; Yang et al., 1986; Shimmield & Price, 1988; Lao et al., 1992; François et al., 1993; Frank et al., 1994; Frank, 1996; Bradtmiller et al., 2014, and their supplemental data). (c) Particulate  $^{231}\text{Pa}$  and  $^{230}\text{Th}$  data obtained in pre-GEOTRACES studies (Cochran et al., 1987; Colley et al., 1995; Guo et al., 1995; Moran et al., 1997, 2001, 2002; Rutgers van der Loeff and Berger, 1993; Vogler et al., 1998; Walter et al., 1997).

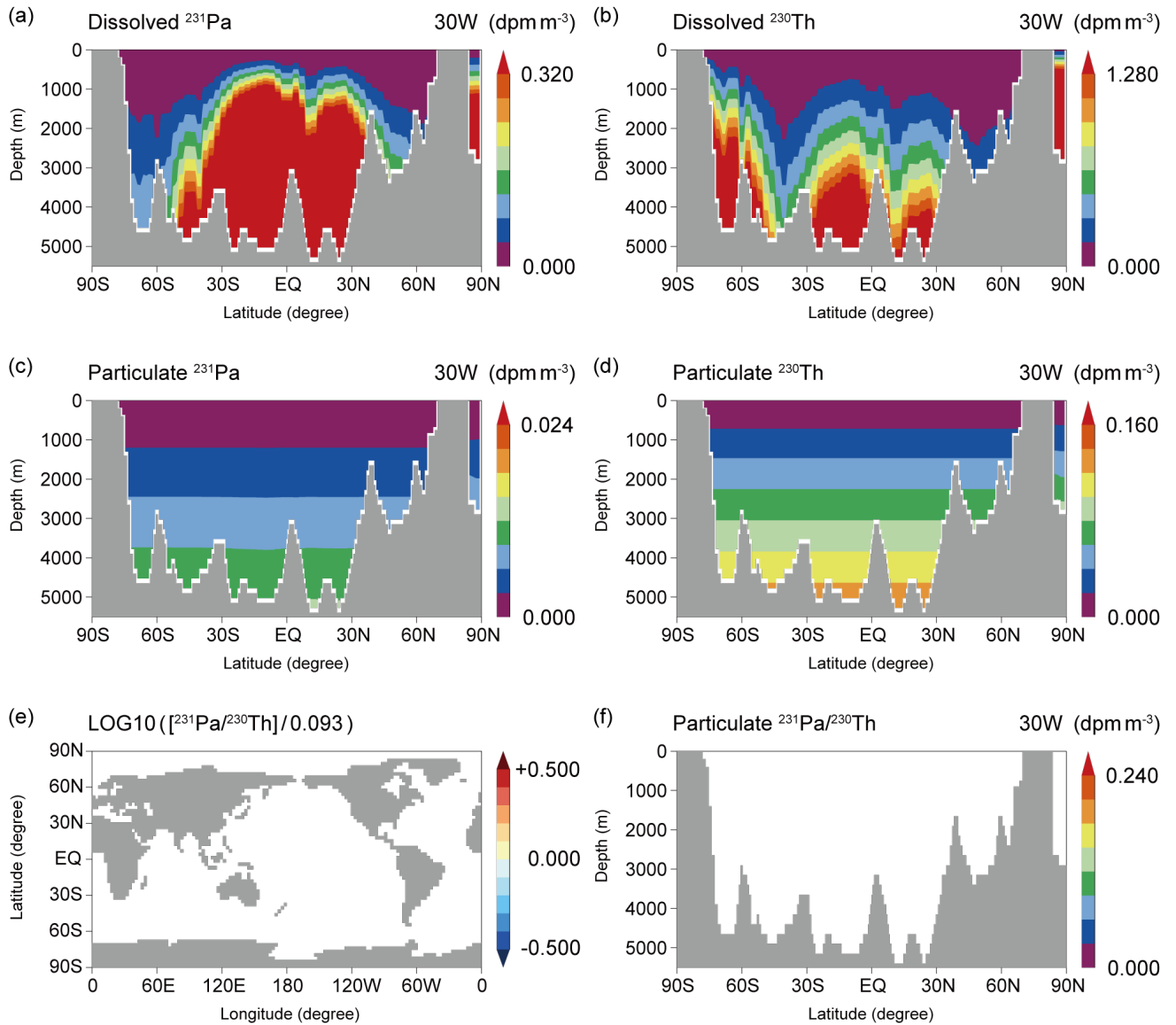


**Figure S2.** (a) Dissolved  $^{231}\text{Pa}$ , (b) dissolved  $^{230}\text{Th}$ , (c) particulate  $^{231}\text{Pa}$ , (d) particulate  $^{230}\text{Th}$ , and (f) particulate  $^{231}\text{Pa}/^{230}\text{Th}$  ratios along  $30^{\circ}\text{W}$  in the Atlantic Ocean in 1D\_EXP. (e) Sedimentary  $^{231}\text{Pa}/^{230}\text{Th}$  ratios normalized by the production ratio of 0.093 in 1D\_EXP.

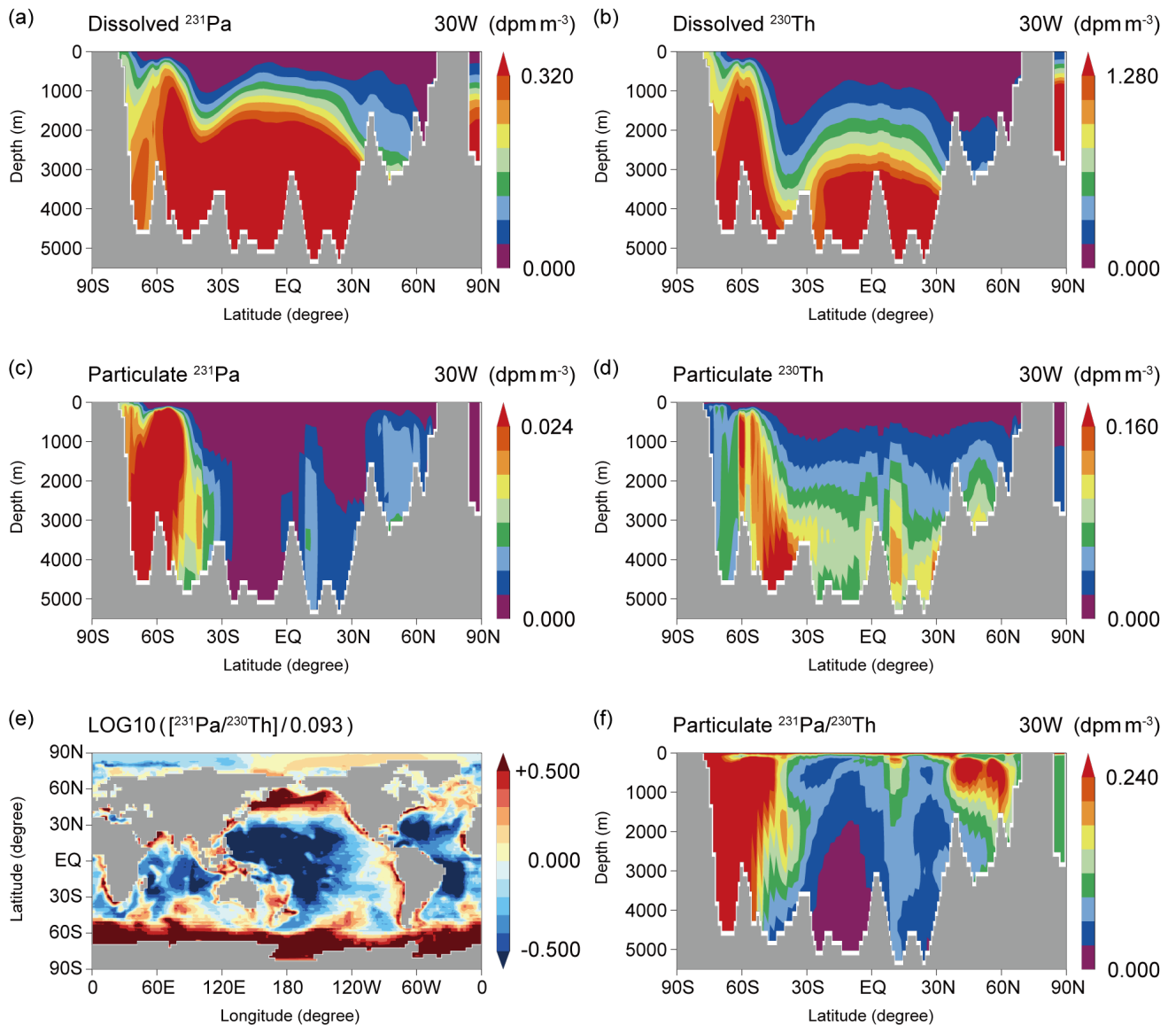


**Figure S3.** The same as Fig. S2 except for 3D\_EXP.

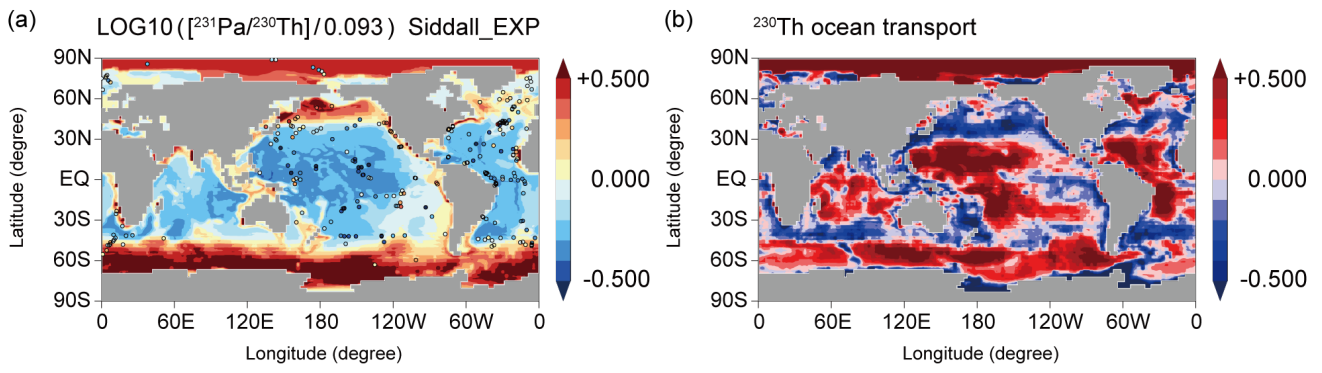


**Figure S4.** (a) Sedimentary  $^{231}\text{Pa}/^{230}\text{Th}$  ratios normalized by the production ratio of 0.093 in Siddall\_EXP. (b) Contributions to the sedimentary  $^{231}\text{Pa}/^{230}\text{Th}$  ratios of Siddell\_EXP from ocean transport solely from  $^{230}\text{Th}$  (i.e.,  $^{231}\text{Pa}(1\text{D})/^{230}\text{Th}(\text{Siddall})$ ).

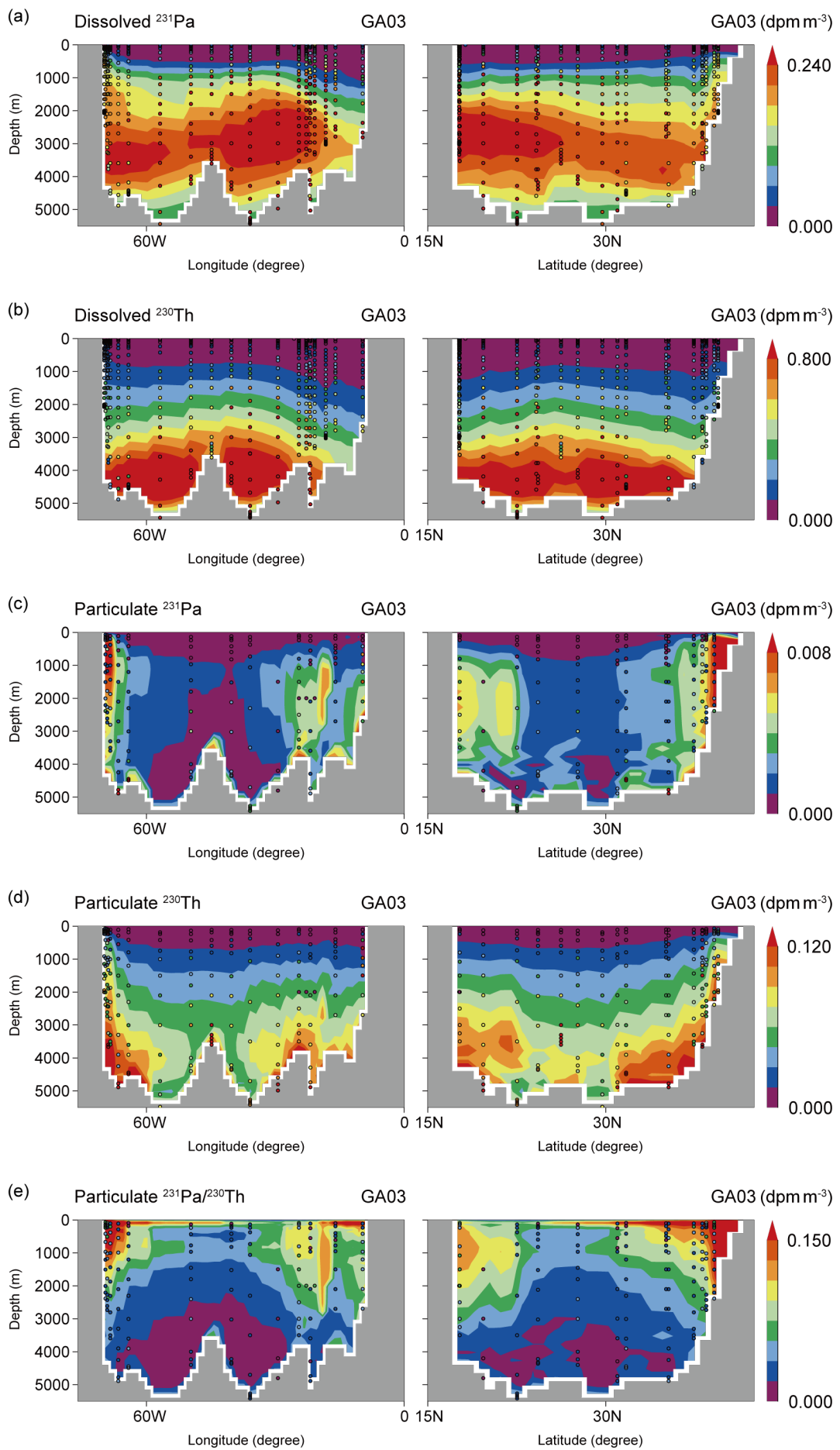


**Figure S5.** (a) Dissolved  $^{231}\text{Pa}$ , (b) dissolved  $^{230}\text{Th}$ , (c) particulate  $^{231}\text{Pa}$ , (d) particulate  $^{230}\text{Th}$ , and (e) particulate  $^{231}\text{Pa}/^{230}\text{Th}$  ratios along the Atlantic GEOTRACES GA03 transect in CTRL\_EXP. The coloured circles represent the GEOTRACES data (GA03; Hayes et al., 2015).

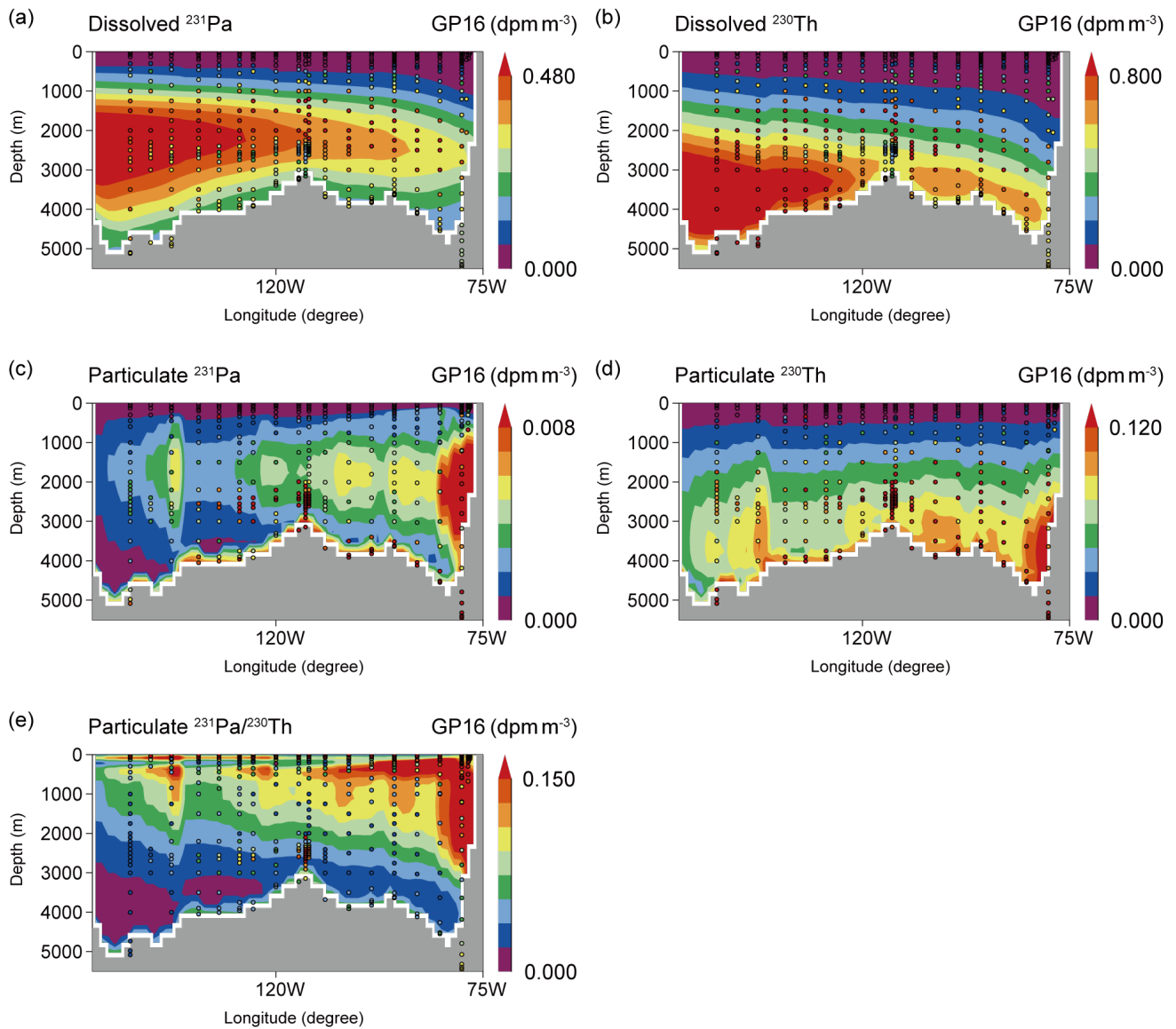


**Figure S6.** (a) Dissolved  $^{231}\text{Pa}$ , (b) dissolved  $^{230}\text{Th}$ , (c) particulate  $^{231}\text{Pa}$ , (d) particulate  $^{230}\text{Th}$ , and (e) particulate  $^{231}\text{Pa}/^{230}\text{Th}$  ratios along the Pacific GEOTRACES GP16 transect in CTRL\_EXP. The coloured circles represent the GEOTRACES data (GP16; Pavia et al., 2018).

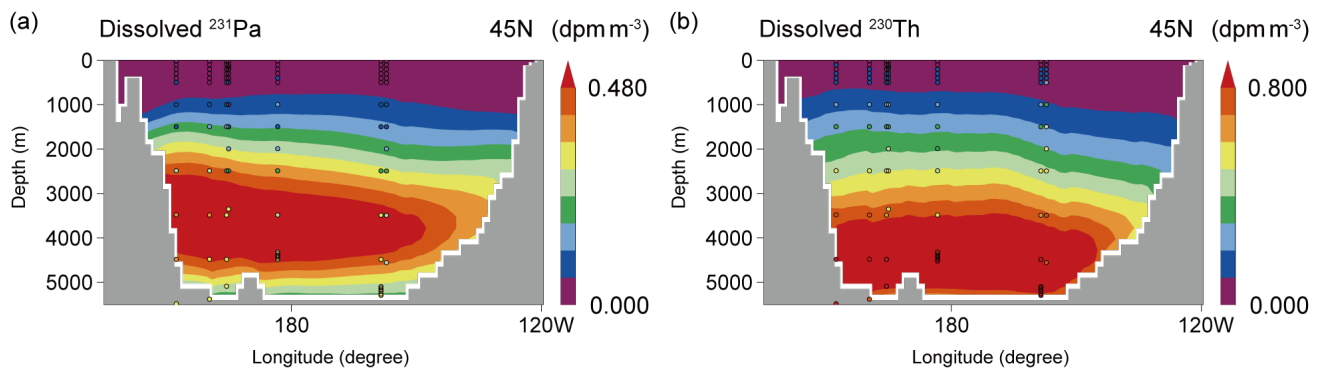


**Figure S7.** (a) Dissolved  $^{231}\text{Pa}$  and (b) dissolved  $^{230}\text{Th}$  along 45°N in the Pacific in CTRL\_EXP. The coloured circles represent the GEOTRACES data (GPc01; Hayes et al., 2013).

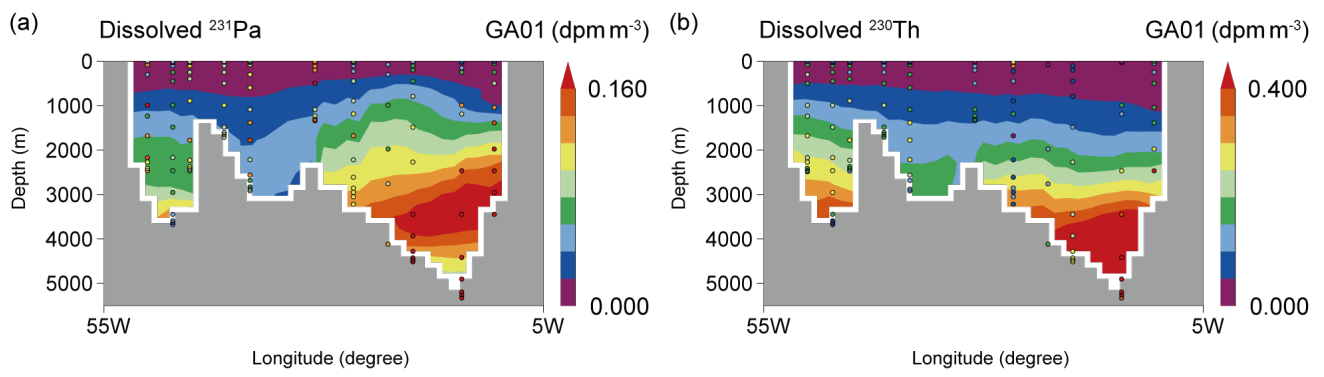


**Figure S8.** (a) Dissolved  $^{231}\text{Pa}$  and (b) dissolved  $^{230}\text{Th}$  along the Atlantic GEOTRACES GA01 transect in CTRL\_EXP. The coloured circles represent the GEOTRACES data (GA01; Deng et al., 2018).

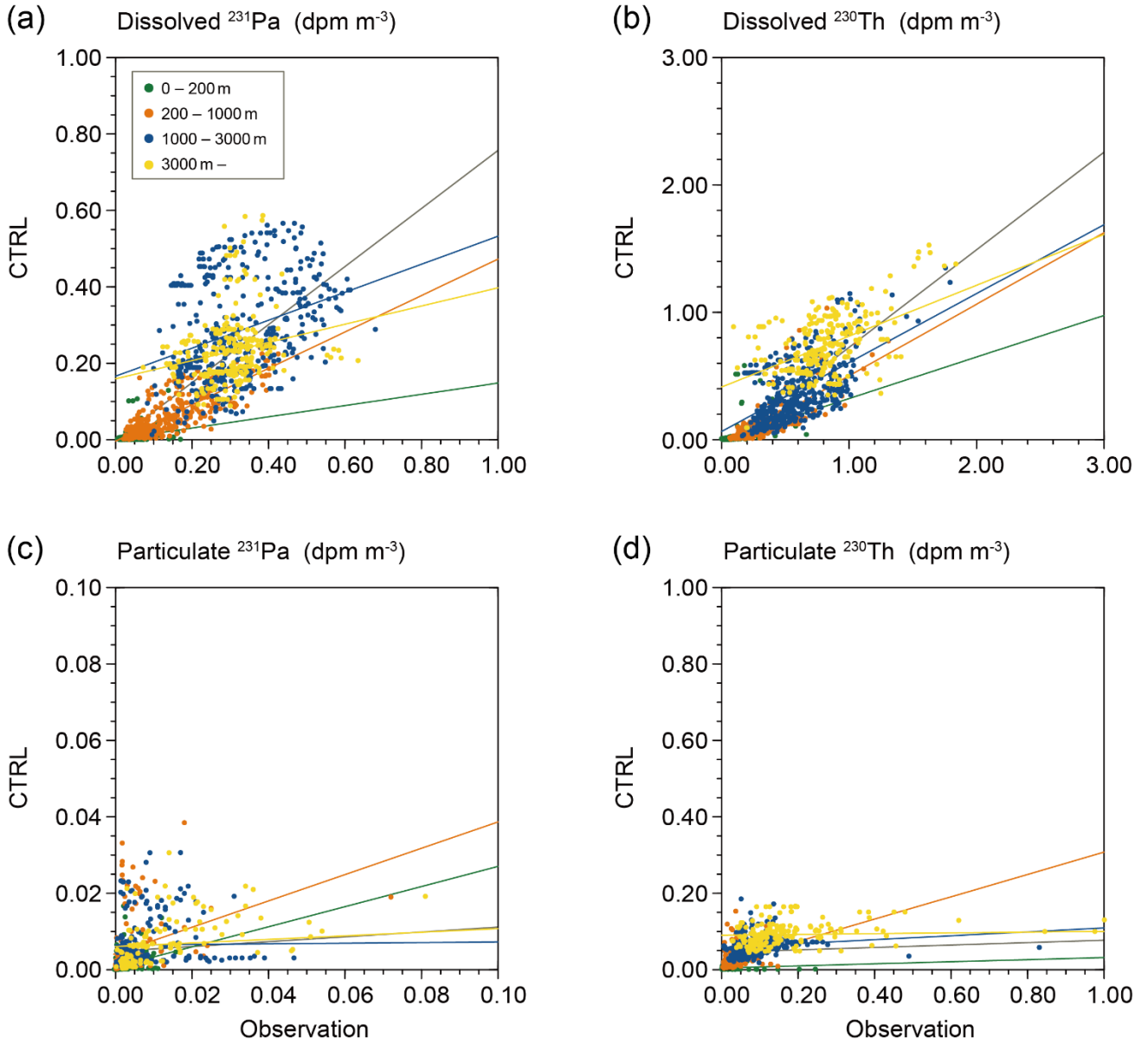


**Figure S9.** The scatter plot of (a) dissolved  $^{231}\text{Pa}$ , (b) dissolved  $^{230}\text{Th}$ , (c) particulate  $^{231}\text{Pa}$ , and (d) particulate  $^{230}\text{Th}$  between CTRL\_EXP and available GEOTRACES data (unit:  $\text{dpm m}^{-3}$ ). Plots from different ocean depth ranges are drawn with different colors: green for 0–200 m, orange for 200–1000 m, blue for 1000–3000m and yellow for deeper than 3000 m. The regression lines are also shown. The gray line represents the linear regression line for all depth ranges. For dissolved  $^{231}\text{Pa}$  and  $^{230}\text{Th}$ , the data from GEOTRACES GA02, GA03, GIPY05, GPc01 and GP16 sections are used. For particulate  $^{231}\text{Pa}$  and  $^{230}\text{Th}$ , the data from GEOTRACES GA03, GIPY05, and GP16 sections are used.

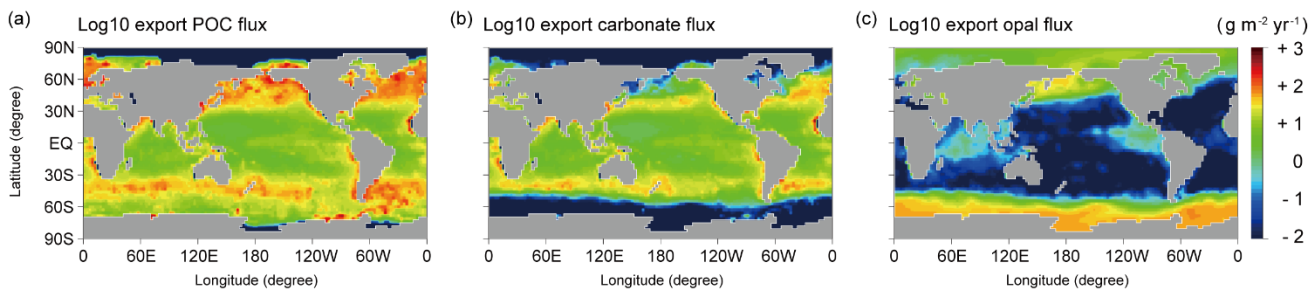


**Figure S10.** Surface particle fluxes (unit:  $\text{g m}^{-2} \text{ yr}^{-1}$ ) of (a) particulate organic carbon, (b) calcium carbonate, and (c) opal.

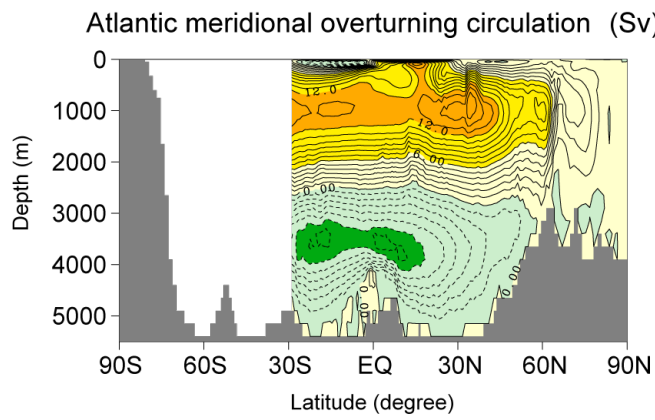


**Figure S11.** Atlantic meridional overturning circulation (AMOC) simulated in the OGCM COCO under modern conditions. The contour interval is 1 Sv ( $1 \text{ Sv} = 10^6 \text{ m}^3 \text{ s}^{-1}$ ).

## References

- Anderson, R. F., Bacon, M. P., and Brewer, P. G.: Removal of  $^{230}\text{Th}$  and  $^{231}\text{Pa}$  from the open ocean, *Earth Planet. Sci. Lett.*, 62(1), 7–23, [https://doi.org/10.1016/0012-821X\(83\)90067-5](https://doi.org/10.1016/0012-821X(83)90067-5), 1983.
- Bradtmiller, L. I., McManus, J. F., and Robinson, L. F.:  $^{231}\text{Pa}/^{230}\text{Th}$  evidence for a weakened but persistent Atlantic meridional overturning circulation during Heinrich Stadial 1, *Nat. Commun.*, 5(1), 5817, <https://doi.org/10.1038/ncomms6817>, 2014.
- Cochran, J. K., Livingston, H. D., Hirschberg, D. J., and Surprenant, L. D.: Natural and anthropogenic radionuclide distributions in the northwest Atlantic Ocean, *Earth Planet. Sci. Lett.*, 84(2–3), 135–152, [https://doi.org/10.1016/0012-821X\(87\)90081-1](https://doi.org/10.1016/0012-821X(87)90081-1), 1987.
- Colley, S., Thomson, J., and Newton, P. P.: Detailed  $^{230}\text{Th}$ ,  $^{232}\text{Th}$  and  $^{210}\text{Pb}$  fluxes recorded by the 1989/90 BOFS sediment trap time-series at  $48^\circ\text{N}$ ,  $20^\circ\text{W}$ , *Deep-Sea Res. I*, 42(6), 833–848, [https://doi.org/10.1016/0967-0637\(95\)00033-3](https://doi.org/10.1016/0967-0637(95)00033-3), 1995.
- Deng F., Henderson, G. M., Castrillejo, M., Perez, F. F., and Steinfeldt, R.: Evolution of  $^{231}\text{Pa}$  and  $^{230}\text{Th}$  in overflow waters of the North Atlantic, *Biogeosciences*, 15, 7299–7313, <https://doi.org/10.5194/bg-15-7299-2018>, 2018.
- François, R., Bacon, M. P., Altabet, M. A., and Labeyrie, L. D.: Glacial/interglacial changes in sediment rain rate in the SW Indian Sector of subantarctic Waters as recorded by  $^{230}\text{Th}$ ,  $^{231}\text{Pa}$ , U, and  $\delta^{15}\text{N}$ , *Paleoceanography*, 8(5), 611–629, <https://doi.org/10.1029/93PA00784>, 1993.
- Frank, M., Eckhardt, J.-D., Eisenhauer, A., Kubik, P. W., Dittrich-Hannen, B., Segl, M., and Mangini, A.: Beryllium 10, thorium 230, and protactinium 231 in Galapagos microplate sediments: Implications of hydrothermal activity and paleoproductivity changes during the last 100,000 years, *Paleoceanography*, 9(4), 559–578, <https://doi.org/10.1029/94PA01132>, 1994.
- Frank, M.: Reconstruction of Late Quaternary environmental conditions applying the natural radionuclides  $^{230}\text{Th}$ ,  $^{10}\text{Be}$ ,  $^{231}\text{Pa}$  and  $^{238}\text{U}$ : a study of deep-sea sediments from the eastern sector of the Antarctic Circumpolar Current System, Ph.D. thesis, Alfred Wegener Institute for Polar and Marine Research, 136 pp., 1996.
- Guo, L., Santschi, P. H., Baskaran, M., and Zindler, A.: Distribution of dissolved and particulate  $^{230}\text{Th}$  and  $^{232}\text{Th}$  in seawater from the Gulf of Mexico and off Cape Hatteras as measured by SIMS, *Earth Planet. Sci. Lett.*, 133(1–2), 117–128, [https://doi.org/10.1016/0012-821X\(95\)00063-I](https://doi.org/10.1016/0012-821X(95)00063-I), 1995.
- Hayes, C. T., Anderson, R. F., Jaccard, S. L., François, R., Fleisher, M. Q., Soon, M., Gersonde, R.: A new perspective on boundary scavenging in the North Pacific Ocean, *Earth Planet. Sci. Lett.*, 369–370, 86–97, <https://doi.org/10.1016/j.epsl.2013.03.008>, 2013.
- Hayes, C. T., Anderson, R. F., Fleisher, M. Q., Huang, K.-F., Robinson, L. F., Lu, Y., Cheng, H., Lawrence Edwards, R., and Bradley Moran, S.:  $^{230}\text{Th}$  and  $^{231}\text{Pa}$  on GEOTRACES GA03, the U.S. GEOTRACES North Atlantic transect, and implications for modern and paleoceanographic chemical fluxes, *Deep-Sea Res. II*, 116, 29–41, <https://doi.org/10.1016/j.dsr2.2014.07.007>, 2015.
- Lao, Y., Anderson, R. F., Broecker, W. S., Trumbore, S. E., Hofmann, H. J., and Wolfli, W.: Transport and burial rates of  $^{10}\text{Be}$  and  $^{231}\text{Pa}$  in the Pacific Ocean during the Holocene period, *Earth Planet. Sci. Lett.*, 113(1–2), [https://doi.org/10.1016/0012-821X\(92\)90218-K](https://doi.org/10.1016/0012-821X(92)90218-K), 1992.
- Mangini, A., and Sonntag, C.:  $^{231}\text{Pa}$  dating of deep-sea cores via  $^{227}\text{Th}$  counting, *Earth Planet. Sci. Lett.*, 37(2), 251–256, [https://doi.org/10.1016/0012-821X\(77\)90170-4](https://doi.org/10.1016/0012-821X(77)90170-4), 1977.

- Moran, S. B., Charette, M. A., Hoff, J. A., Edwards, R. L., and Landing, W. M.: Distribution of 230Th in the Labrador Sea and its relation to ventilation, *Earth Planet. Sci. Lett.*, 150(1–2), 151–160, [https://doi.org/10.1016/s0012-821x\(97\)00081-2](https://doi.org/10.1016/s0012-821x(97)00081-2), 1997.
- Moran, S. B., Shen, C.-C., Weinstein, S. E., Hettinger, L. H., Hoff, J. H., Edmonds, H. N., and Edwards, R. L.: Constraints on deep water age and particle flux in the equatorial and South Atlantic Ocean based on seawater 231Pa and 230Th data, *Geophys. Res. Lett.*, 28(18), 3437–3440, <https://doi.org/10.1029/2001GL013339>, 2001
- Moran, S. B., Shen, C. C., Edmonds, H. N., Weinstein, S. E., Smith, J. N., and Edwards, R. L.: Dissolved and particulate 231Pa and 230Th in the Atlantic Ocean: Constraints on intermediate/deep water age, boundary scavenging, and 231Pa/230Th fractionation, *Earth Planet. Sci. Lett.*, 203(3–4), 999–1014, [https://doi.org/10.1016/S0012-821X\(02\)00928-7](https://doi.org/10.1016/S0012-821X(02)00928-7), 2002.
- Müller, P. J., and Mangini, A.: Organic carbon decomposition rates in sediments of the pacific manganese nodule belt dated by 230Th and 231Pa, *Earth Planet. Sci. Lett.*, 51(1), 94–114, [https://doi.org/10.1016/0012-821X\(80\)90259-9](https://doi.org/10.1016/0012-821X(80)90259-9), 1980.
- Pavia, F., Anderson, R., Vivancos, S., Fleisher, M., Lam, P., Lu, Y., Cheng, H., Zhang, P., Lawrence Edwards, R.: Intense hydrothermal scavenging of 230Th and 231Pa in the deep Southeast Pacific, *Mar. Chem.*, 201, 212–228, <https://doi.org/10.1016/J.MARCHEM.2017.08.003>, 2018.
- Rutgers van der Loeff, M. M., and Berger, G. W.: Scavenging of 230Th and 231Pa near the antarctic polar front in the South Atlantic, *Deep-Sea Res. I*, 40(2), 339–357, [https://doi.org/10.1016/0967-0637\(93\)90007-P](https://doi.org/10.1016/0967-0637(93)90007-P), 1993.
- Schlitzer, R., Anderson, R. F., Dodds, E. M., Lohan, M., Geibert, W., Tagliabue, A., Bowie, A., Jeandel, C., Maldonado, M. T., Landing, W. M., Cockwell, D. et al.: The GEOTRACES Intermediate Data Product 2017, *Chem. Geol.*, 493, 210–223, <https://doi.org/10.1016/j.chemgeo.2018.05.040>, 2018.
- Schmitz, W., Mangini, A., Stoffers, P., Glasby, G. P., and Plüger, W. L.: Sediment accumulation rates in the southwestern Pacific Basin and Aitutaki Passage, *Mar. Geol.*, 73(1–2), 181–190, [https://doi.org/10.1016/0025-3227\(86\)90118-0](https://doi.org/10.1016/0025-3227(86)90118-0), 1986.
- Shimmield, G. B., Murray, J. W., Thomson, J., Bacon, M. P., Anderson, R. F., and Price, N. B.: The distribution and behaviour of 230Th and 231Pa at an ocean margin, Baja California, Mexico, *Geochim. Cosmochim. Acta*, 50(11), 2499–2507, [https://doi.org/10.1016/0016-7037\(86\)90032-3](https://doi.org/10.1016/0016-7037(86)90032-3), 1986.
- Shimmield, G. B., and Price, N. B.: The scavenging of U, 230Th and 231Pa during pulsed hydrothermal activity at 20°S, East Pacific Rise, *Geochim. Cosmochim. Acta*, 52(3), 669–677, [https://doi.org/10.1016/0016-7037\(88\)90329-8](https://doi.org/10.1016/0016-7037(88)90329-8), 1988.
- Vogler, S., Scholten, J., Rutgers van der Loeff, M., and Mangini, A.: 230Th in the eastern North Atlantic: The importance of water mass ventilation in the balance of 230Th, *Earth Planet. Sci. Lett.*, 156(1–2), 61–74, [https://doi.org/10.1016/s0012-821x\(98\)00011-9](https://doi.org/10.1016/s0012-821x(98)00011-9), 1998.
- Walter, H. J., Rutgers van der Loeff, M. M., and Hoeltzen, H.: Enhanced scavenging of 231Pa relative to 230Th in the South Atlantic south of the Polar Front: Implications for the use of the 231Pa/230Th ratio as a paleoproductivity proxy, *Earth Planet. Sci. Lett.*, 149(1–4), 85–100, [https://doi.org/10.1016/s0012-821x\(97\)00068-x](https://doi.org/10.1016/s0012-821x(97)00068-x), 1997.
- Yang, H.-S., Nozaki, Y., Sakai, H., and Masuda, A.: The distribution of 230Th and 231Pa in the deep-sea surface sediments of the Pacific Ocean, *Geochim. Cosmochim. Acta*, 50(1), 81–89, [https://doi.org/10.1016/0016-7037\(86\)90050-5](https://doi.org/10.1016/0016-7037(86)90050-5), 1986.